polymers

MDPI

Article

Rational Designing of NiO Nanoparticles Anchored with PEG-WO_3 for Enhanced Water Oxidation Performance

Mrunal Bhosale, Pritam J. Morankar, Rutuja U. Amate and Chan-Wook Jeon *

School of Chemical Engineering, Yeungnam University, 280 Daehak-ro, Gyeongsan 712-749, Republic of Korea; mrunal.snst.1@gmail.com (M.B.); pritam.nanoworld@gmail.com (P.J.M.); rutu.nanoworld@gmail.com (R.U.A.)
* Correspondence: cwjeon@ynu.ac.kr

Abstract: The electrochemical water splitting method is widely regarded as an efficient and sustainable approach for producing high-purity hydrogen in an environmentally friendly manner. Cost-effective and efficient electrocatalysts are essential for augmenting the electrocatalytic water oxidation reaction. Herein, the PEG-WO_3-NiO electrocatalyst is acknowledged for attaining efficient oxygen evolution reaction (OER) performances in alkaline conditions. The NiO nanoparticles anchored themselves to the PEG-WO_3's surface and produced an effective interfacial contact between the electrocatalyst materials. Among various compositions, the optimized ratio of the PEG-WO_3-NiO electrocatalyst exhibits a low overpotential of 349.7 mV at a current density of 10 mA cm^{-2} and a Tafel slope of 71.22 mV dec^{-1} for the OER in 1 M KOH. Additionally, the electrocatalyst demonstrates excellent stability, maintaining its performance even after 5000 cyclic voltammetry (CV) cycles and chronopotentiometry analysis. Given its durability and high electrochemically active surface area, the PEG-WO_3-NiO electrocatalyst contributes to the advancement of cost-effective and scalable solutions for water oxidation applications.

Keywords: electrochemical water splitting; oxygen evolution reaction; hydrogen evolution reaction; electrocatalyst; charge transfer

Academic Editors: Shin-Ichi Yusa and Arunas Ramanavicius

Received: 29 March 2025
Revised: 19 April 2025
Accepted: 26 April 2025
Published: 7 May 2025

Citation: Bhosale, M.; Morankar, P.J.; Amate, R.U.; Jeon, C.-W. Rational Designing of NiO Nanoparticles Anchored with PEG-WO_3 for Enhanced Water Oxidation Performance. *Polymers* **2025**, *17*, 1281. https://doi.org/10.3390/polym17091281

1. Introduction

In the last few years, growing environmental concerns associated with the extensive utilization and reliance on fossil fuels have driven a global shift towards renewable energy sources, including solar, wind, and tidal energy. These green alternatives are increasingly regarded as viable solutions to address the ongoing energy crisis while mitigating pollution and reducing carbon emissions [1–3]. Among the various strategies for sustainable energy production, electrochemical water splitting has emerged as a highly promising approach for generating high-purity hydrogen, which serves as an efficient and clean fuel with broad industrial applications [4,5]. Water electrolysis is fundamentally governed by two critical half-reactions, i.e., the hydrogen evolution reaction (HER) and the oxygen evolution reaction (OER). These reactions require highly efficient electrocatalysts to lower the activation energy and enhance the overall energy conversion efficiency. In the field of water splitting, noble metal-based materials have long been recognized as benchmark electrocatalysts due to their exceptional catalytic activity and stability. Specifically, IrO_2 and RuO_2 exhibit superior OER activity, while Pt- and Pd-based catalysts are widely regarded for their outstanding HER performance. However, the widespread industrial implementation of these noble metal catalysts is significantly constrained by their high cost and limited natural abundance [6–8]. This has encouraged widespread research into

developing cost-effective and earth-abundant alternative materials with comparable or superior electrocatalytic performance.

Transition metal-based catalysts, including those derived from nickel, cobalt, and iron, as well as heterostructured and nanostructured materials have demonstrated great potential in addressing these challenges. Tungsten oxide (WO_3) exhibits a tunable crystalline phase and a highly adaptable structure, allowing for the precise modulation of its catalytic performance through structural engineering and surface electronic modifications [9–11]. Conversely, the widespread application of tungsten oxide in electrocatalysis is constrained by several inherent limitations, including its adequate catalytic activity, limited density of active sites, and low intrinsic electronic conductivity [10,12–14]. These challenges hinder its overall efficiency and necessitate further advancements in material design and surface engineering to enhance its electrocatalytic performance [10,12]. Various effective strategies have been developed to optimize these characteristics, thus enhancing its electrocatalytic efficiency. Moreover, tungsten oxide-based materials have garnered significant research interest due to their ease of synthesis and remarkable stability in extreme pH conditions. These combined properties position tungsten oxide as a highly promising candidate for water electrocatalysis [9]. Nickel-based electrocatalysts have gained significant attention in alkaline electrochemical systems due to their superior catalytic activity which can be attributed to their high density of active sites and unique electronic and structural properties [15–17]. Additionally, nickel exhibits excellent electrochemical stability under alkaline conditions, further contributing to its effectiveness as an electrocatalyst. The integration of nickel compounds into hybrid electrocatalysts offers multiple advantages, leading to significant improvements in overall electrochemical performance. This enhancement arises from the following three key factors: (i) the inherent OER activity of nickel, which accelerates reaction kinetics; (ii) improved charge transfer efficiency; and (iii) the formation of strong interfacial interactions that generate synergistic effects resulting in enhanced structural integrity and catalytic stability [16,18]. Recent developments have recognized NiO nanostructures as highly promising electrocatalysts for the OER. Their advantages include fast electrochemical response, excellent corrosion resistance, natural abundance, cost-effectiveness, improved surface kinetics, and long-term stability [19,20]. For example, in a 1 M KOH electrolyte, zero-dimensional (0D) NiO nanoparticles demonstrated an overpotential of 373 mV at a current density of 10 mA cm^{-2}. In contrast, two-dimensional (2D) porous NiO nanoplates exhibited a higher overpotential of 476 mV under identical conditions, indicating the influence of morphological differences on OER performance [21]. The NiO hollow spheres calcined at 300 °C (NiO-300) exhibited notable bifunctional electrocatalytic activity for both the OER and HER in 1 M KOH. NiO-300 required an overpotential of 424 mV for HER and 370 mV for OER to achieve a current density of 10 mA cm^{-2}, highlighting its efficiency as a dual-functional electrocatalyst [22]. The Ag_2O–NiO nanostructures exhibit remarkable electrocatalytic performance, requiring an overpotential of 140 mV for the HER and 430 mV for the OER at 10 mA cm^{-2}. Additionally, the Ag_2O/NiO composite demonstrates outstanding long-term stability maintaining efficient OER and HER activity over an extended operational period [23].

In this study, we synthesized PEG-WO_3-NiO nanostructured electrocatalysts and demonstrated their enhanced electrocatalytic performance for the alkaline OER. The incorporation of NiO with PEG-WO_3 was aimed at boosting the catalytic activity. Spectroscopic analyses confirmed the successful formation of the PEG-WO_3-NiO nanocomposite, with NiO nanoparticles uniformly anchored on the PEG-WO_3 surface. Among the various compositions tested, $PWNiO_{1.5}$ exhibited the most favorable electrochemical characteristics, showing a low overpotential of 349.7 mV at a current density of 10 mA cm^{-2} and a Tafel slope of 71.22 mV·dec^{-1}. The PEG-WO_3-NiO catalyst significantly enhances the transfer of

active species and improves electrocatalytic performance primarily due to its increased active surface area and synergistic effects. Furthermore, the stability of the electrocatalyst was confirmed through extended cyclic voltammetry and chronopotentiometry measurements.

2. Experimental Section

2.1. Chemicals

Nickel nitrate hexahydrate ($Ni(NO_3)_2 \cdot 6H_2O$), sodium tungstate dihydrate ($Na_2WO_4 \cdot 2H_2O$, ≥99%), poly(ethylene glycol) (PEG), polyvinylidene fluoride (PVDF), and N-methyl-2-pyrrolidone (NMP, ≥99%) were procured from Sigma-Aldrich, St. Louis, MO, USA. Hydrochloric acid (HCl, extra pure) and ethanol (EtOH, C_2H_5OH, 94.5%) were sourced from Duksan Chemicals, Gyeonggi-do, Republic of Korea. Potassium hydroxide (KOH, >85%) was supplied by Daejung Chemicals & Metals, Gyeonggi-do, Republic of Korea. Acetylene black (99.9+%) was obtained from Thermo Scientific, Seoul, Republic of Korea. The carbon cloth utilized in this study was acquired from NARA Cell-Tech Corporation, Seoul, Republic of Korea. All chemicals were used without further purification, and deionized (DI) water was exclusively employed in all experimental procedures to ensure consistency and reliability in the study.

2.2. Preparation of PEG-WO_3-NiO

The synthesis of the PEG-WO_3-NiO nanostructures was conducted via a hydrochloric acid-assisted precipitation technique, as depicted in Figure 1. Initially, $Na_2WO_4 \cdot 2H_2O$ was dissolved in 50 mL of DI water under continuous stirring for 30 min to achieve complete dissolution. Subsequently, diluted HCl was incrementally introduced into the homogeneous solution until the pH reached approximately 2. Following pH adjustment, 3% PEG was incorporated and stirred for an additional 30 min to ensure complete dissolution. Once the PEG was fully dissolved, varying concentrations (0.5, 1, and 1.5%) of $Ni(NO_3)_2 \cdot 6H_2O$ were introduced into the solution. The mixture underwent vigorous stirring for a further 2 h before being left undisturbed overnight to facilitate precipitation. After the precipitation process, the supernatant was carefully decanted, and the resulting precipitate was thoroughly washed and subsequently dried at 120 °C for 3 h. The dried material was then subjected to thermal annealing at 450 °C for 3 h, followed by grinding using an agate mortar and pestle to obtain the final nanostructured product. The PEG-WO_3-NiO composite was made with three different concentrations of $Ni(NO_3)_2.6H_2O$ (0.5, 1, and 1.5%), designated as $PWNiO_{0.5}$, $PWNiO_1$, and $PWNiO_{1.5}$, respectively.

2.3. Material Characterization

The structural properties of the synthesized nanomaterials were examined using an X-ray diffractometer (X'Pert Pro, PAN Analytical, Almelo, The Netherlands) equipped with a Cu Kα radiation source. Raman spectroscopy was carried out with an XploRA Plus system (HORIBA Jobin Yvon S.A.S, Paris, France) to analyze the vibrational characteristics. The surface chemical composition and oxidation states were investigated through X-ray photoelectron spectroscopy (XPS) using a Thermo Scientific K-Alpha surface, Cheshire, UK analysis system. Additionally, the surface morphology, particle size distribution, elemental composition, and elemental mapping were evaluated using scanning electron microscopy (SEM, HITACHI S-4800, Tokyo, Japan) integrated with an energy-dispersive X-ray (EDX) analysis system and high-resolution transmission electron microscopy (HRTEM, Tecnai F21, FEI Company, Tokyo, Japan).

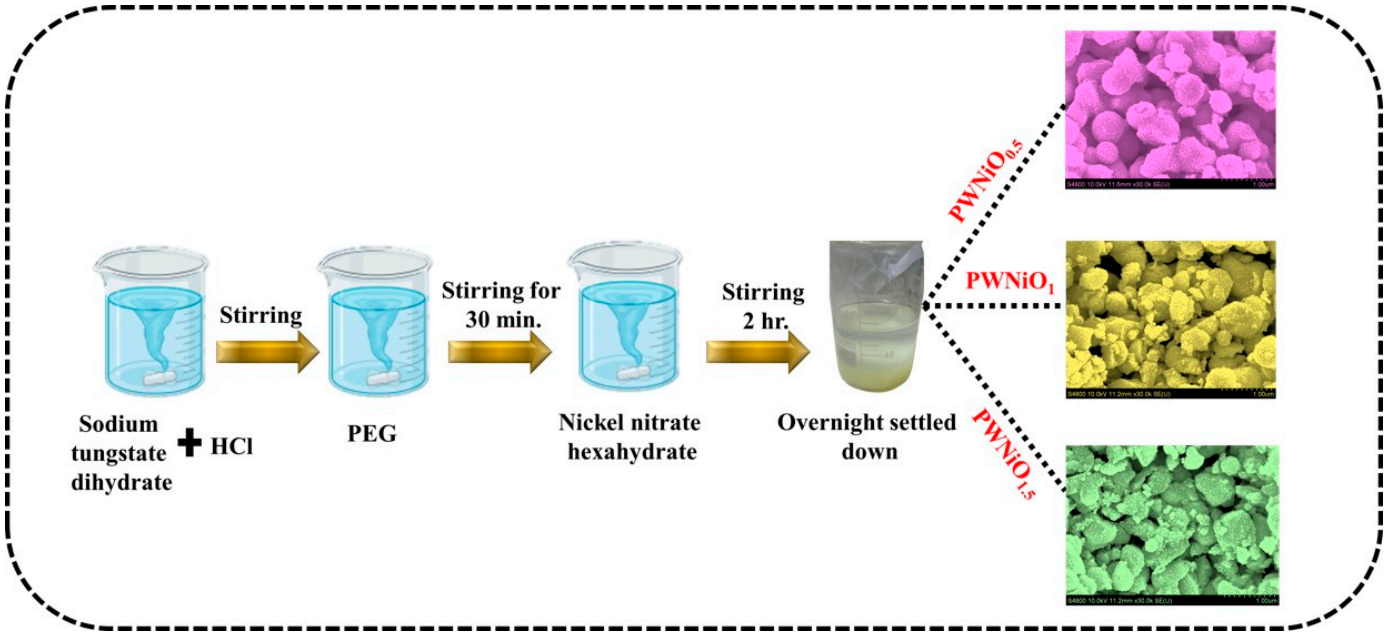

Figure 1. Schematic illustration of synthesis of the PEG-WO_3-NiO nanocomposites.

2.4. Electrochemical Analysis

A Biologic Instrument WBCS3000 battery cycler, Gières, France was used to perform electrochemical measurements. A three-electrode arrangement was employed for comprehensive analysis. Prior to coating the electrocatalyst onto carbon cloth (CC) the substrate underwent a pre-treatment process involving sequential sonication in 1 M HCl, DI water, and ethanol for 20 min each, followed by drying at 70 °C overnight. The electrocatalyst paste was formulated with an 80:10:10 weight ratio of active material, PVDF, and acetylene black using NMP as the solvent. The prepared slurry was uniformly coated onto pre-treated 1 × 1 cm^2 carbon cloth and dried at 60 °C overnight to ensure proper adhesion. For electrochemical characterization, the coated carbon cloth functioned as the working electrode, while a Hg/HgO electrode and a platinum plate functioned as the reference and counter electrodes, respectively. All electrochemical measurements were carried out in a N_2-saturated 1 M KOH electrolyte solution. Cyclic voltammetry (CV) was analyzed in the non-Faradaic region within a potential range of 0.1 to 0.2 V at varying scan rates of 5, 10, 15, 20, and 25 mV s^{-1}. The ECSA was subsequently calculated using the following equation [24]:

$$ECSA = \frac{C_{dl}}{C_s} \quad (1)$$

where C_{dl} signifies the electrochemical double-layer capacitance, while C_s indicates the specific capacitance of a planar surface in a 1 M KOH electrolyte, which is reported to be 0.040 mF cm^{-2} [25,26]. To determine the overpotential for the OER, linear sweep voltammetry (LSV) was conducted at a scan rate of 5 mV s^{-1} within a potential range of 0 to 1 V. All electrochemical measurements were performed using the Hg/HgO reference electrode, and the attained data were converted to the reversible hydrogen electrode (RHE) scale using the Nernst equation, as follows:

$$E_{RHE} = E_{Hg/HgO} + E^{\circ}{}_{Hg/HgO} + 0.0591 \times (pH) \quad (2)$$

where $E^{\circ}{}_{Hg/HgO}$ represents the standard electrode potential of the Hg/HgO reference electrode, and the pH of a 1 M KOH solution is approximately 13.9.

LSV was utilized to relate the optimized electrocatalysts stability before and after 5000 cycles of CV study.

3. Result and Discussion

The structural integrity, crystallinity, and phase purity of the synthesized materials were thoroughly examined using X-ray diffraction (XRD) analysis. Figure 2a presents the XRD spectra of $PWNiO_{0.5}$, $PWNiO_1$, and $PWNiO_{1.5}$ composites providing critical insights into their phase composition. The diffraction pattern of WO_3 exhibits distinct peaks at 23.5°, 28.8°, 33.5°, 54.2°, and 60.0° which correspond to the (110), (101), (111), (221), and (311) crystal planes, respectively. These peak positions align well with the standard diffraction data from the JCPDS card No. 01-085-0808, confirming the successful formation of WO_3 with its characteristic crystalline structure. Additionally, the presence of nickel oxide within the composite is indicated by prominent diffraction peaks observed at 37.2°, 43.2°, and 62.5° which are attributed to the (101), (012), and (110) lattice planes, respectively. The NiO phase exhibits a rhombohedral crystal structure consistent with JCPDS card No. 01-044-1159 [27,28]. A noticeable trend in the XRD patterns reveals that as the concentration of nickel increases, the intensity of the corresponding diffraction peaks also intensifies further validating the successful incorporation of nickel into the composite matrix. These findings confirm the successful formation of the PEG-WO_3-Ni nanocomposite with well-defined crystallinity and phase purity. The structural characteristics as revealed by XRD support the potential applicability of this composite in electrocatalytic processes where well-crystallized phases contribute to enhanced catalytic activity and stability. To examine the molecular interactions within the PEG-WO_3-NiO nanocomposites, Raman scattering analysis was performed, as illustrated in Figure 2b. The $PWNiO_{1.5}$ nanocomposite exhibited distinct Raman peaks at 129, 264, 318, 414, 699, and 808 cm^{-1}. The peak observed at 129 cm^{-1} corresponds to the antisymmetric stretching vibrations of O–W–O bonds [12]. The bending vibrational modes associated with the O–W–O bridging bonds were identified at 264 and 318 cm^{-1} [29,30]. Additionally, the peaks appearing at 699 and 808 cm^{-1} are characteristic of the WO_3 corresponding to W–O stretching vibrations [12]. Furthermore, the Raman peak detected at 414.3 cm^{-1} is attributed to the Ni–O stretching mode, indicating the presence of NiO species [31,32].

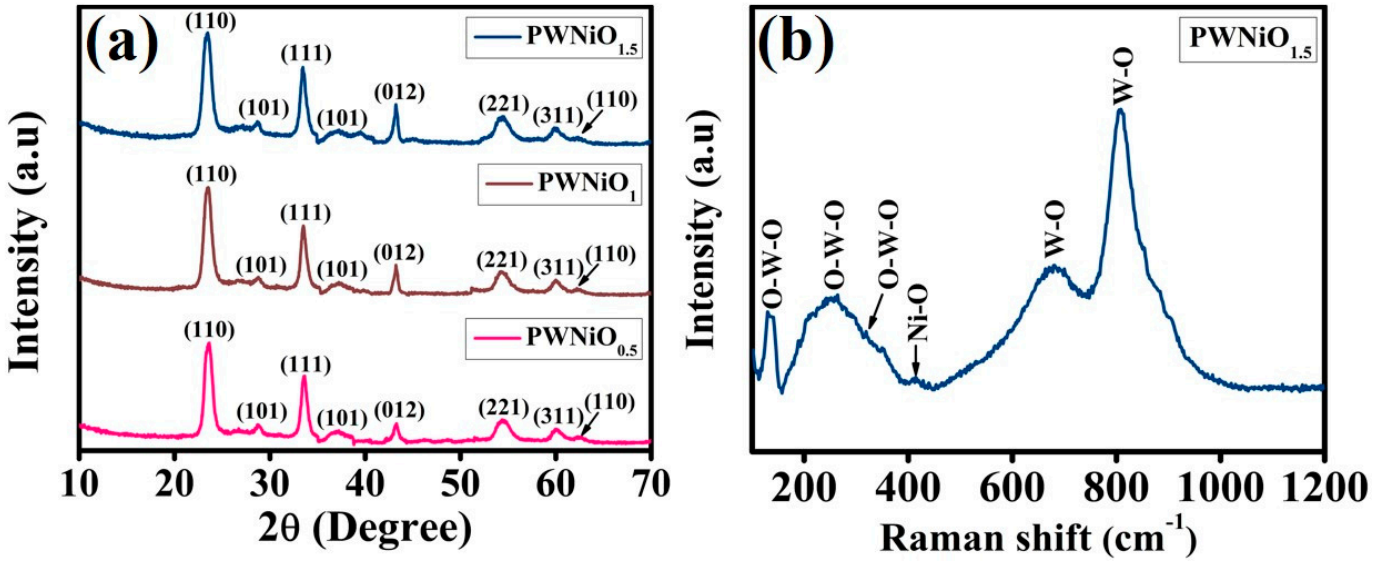

Figure 2. (**a**) XRD spectra of all the composites and (**b**) Raman spectra of the $PWNiO_{1.5}$ composite.

The surface chemical composition and valence states of tungsten (W), oxygen (O), and nickel (Ni) in the $PWNiO_{1.5}$ nanocomposite were analyzed using X-ray photoelectron spectroscopy (XPS). The full XPS survey spectrum (Figure 3a) confirms the presence of W, O, and Ni elements within the composite. To further elucidate the chemical states of these elements, the XPS spectra were deconvoluted, and the high-resolution spectra of W4f, O1s, and Ni2p are presented in Figure 3b,c,d, respectively. The deconvoluted W4f spectrum (Figure 3b) exhibits two distinct peaks at binding energies of 35.4 eV and 37.5 eV, corresponding to the $4f_{7/2}$ and $4f_{5/2}$ orbitals of W^{6+} in the WO_3 phase, respectively [33–35]. The high-resolution O1s spectrum (Figure 3c) reveals a peak at 530.0 eV that is attributed to W–O bonds in WO_3 [34]. One additional peak is present at 531.3 eV which shows Ni–O bonding in the $PWNiO_{1.5}$ composite [28,36]. The Ni2p's high-resolution spectrum (Figure 3d) was deconvoluted into four characteristic peaks. The peak at 855.8 eV corresponds to $Ni2p_{3/2}$, while the satellite peak associated with $Ni2p_{3/2}$ appears at 861.5 eV [23,37]. Another peak at 873.6 eV is assigned to $Ni2p_{1/2}$, with an additional shake-up satellite peak observed at 879.5 eV [23]. These spectral features indicate the presence of a NiO structure, suggesting the partial oxidation of Ni^{2+} species within the composite.

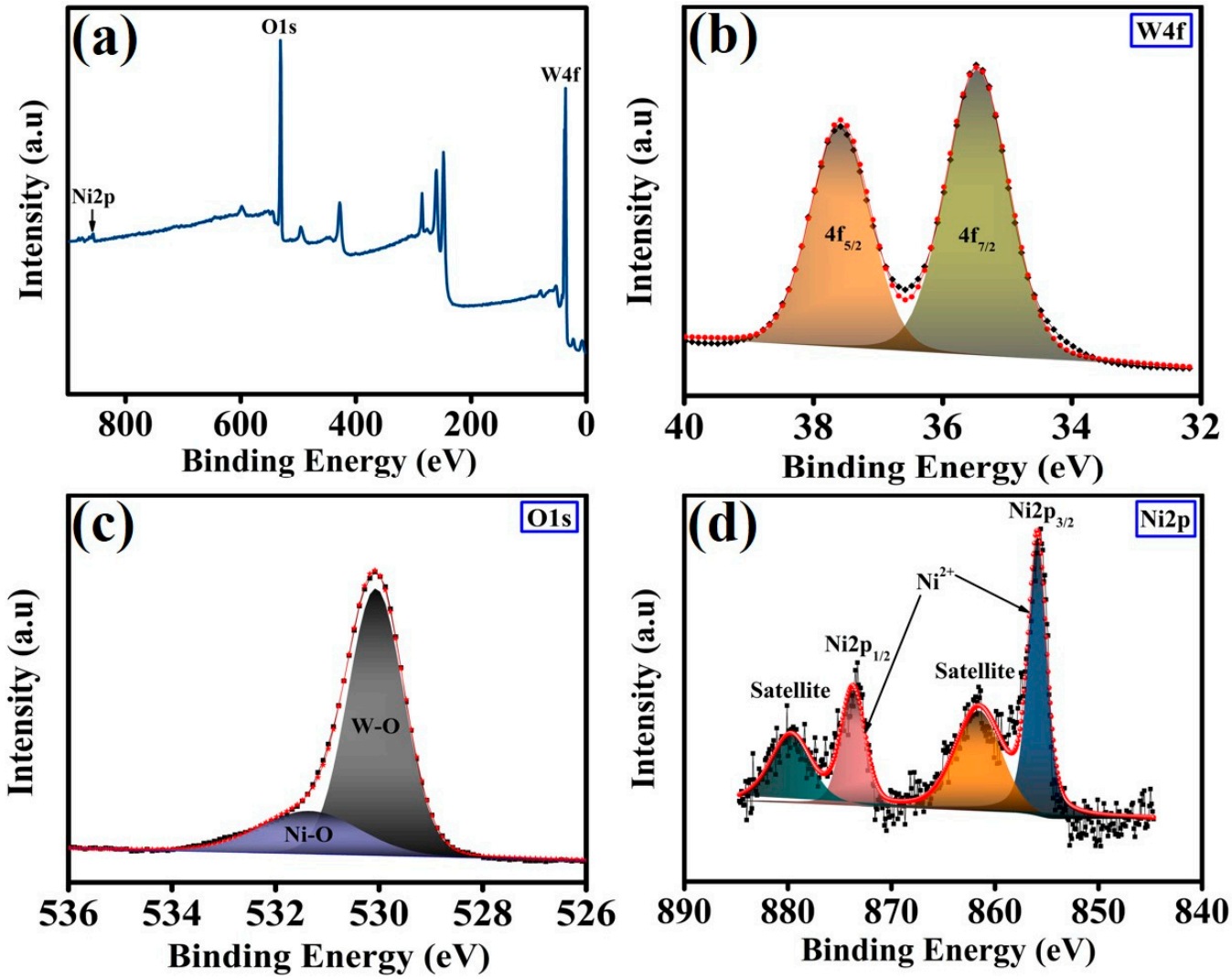

Figure 3. (**a**) High-resolution XPS spectra, (**b**) W4f, (**c**) O1s, and (**d**) Ni2p spectra of $PWNiO_{1.5}$ composite.

The morphological features and elemental configuration of the synthesized electrocatalyst materials were investigated using scanning electron microscopy (SEM) and energy-dispersive X-ray spectroscopy (EDAX). Figure S1 and Figure 4 depict the morphological

variations in WO_3 and PEG-WO_3-NiO composites with different compositions, respectively. SEM analysis of WO_3 (Figure S1a,b) reveals an interconnected nanogranular structure with a droplet-like morphology. Upon the incorporation of PEG, a noticeable increase in nanogranular size is observed in the $PWNiO_{0.5}$, $PWNiO_1$, and $PWNiO_{1.5}$ composites. The nickel oxide component is present in a nanoparticle-like structure. However, in the $PWNiO_{0.5}$ (Figure 4(a1,a2)) its distribution appears relatively low which may limit its overall catalytic effectiveness. In the case of $PWNiO_1$ (Figure 4(b1,b2)) and $PWNiO_{1.5}$ (Figure 4(c1,c2)) an increase in NiO nanoparticle formation is observed with a higher Ni content. Notably, in the $PWNiO_{1.5}$ composite, NiO nanoparticles are well attached to the PEG-WO_3 matrix, exhibiting a uniform distribution. Elemental composition analysis of the $PWNiO_{1.5}$ composite was performed using EDAX, as presented in Figure 4(d1,d2). The analysis confirms the presence of W, O, and Ni, with their respective weight percentages determined as 75.59%, 18.11%, and 6.31%. To evaluate the uniformity of the elemental distribution, EDAX mapping was conducted as illustrated, in Figure 4(e1–e4). The mapping results indicate a homogeneous dispersion of NiO nanoparticles throughout the PEG-WO_3 matrix. This uniform distribution suggests that enhanced electrocatalytic performance can be achieved by facilitating effective interaction between the active sites, which may contribute to improved catalytic activity. The morphological and structural characteristics of the synthesized $PWNiO_{1.5}$ composite were further elucidated through high-resolution transmission electron microscopy (HRTEM), as shown in Figure S2a,b. The HRTEM image reveals a densely packed structure composed of PEG assisted WO_3 nanogranules with uniformly dispersed NiO nanoparticles. The nanogranular morphology of the WO_3 is evident, forming a constant and interconnected network. The darker contrast spots correspond to the higher electron-dense NiO nanoparticles embedded on the PEG-WO_3 nanogranulars. The NiO nanoparticles marked with yellow squares are seen to be well-dispersed, suggesting effective confinement within the PEG-WO_3 framework during synthesis.

The evaluation of catalytic activity in an alkaline medium is conventionally determined by monitoring oxygen evolution. A key parameter in assessing the efficiency of electrocatalysts is the overpotential at a specified current density, as it directly influences catalytic performance [38]. Consequently, comprehensive electrochemical characterization were conducted to analyze the OER activity. The electrochemical assessments were performed using a three-electrode configuration, where the synthesized materials were deposited onto carbon cloth as the working electrode while Hg/HgO and a platinum plate functioned as the reference and counter electrodes, respectively. Linear sweep voltammetry (LSV) measurements were carried out in a 1 M KOH electrolyte at a scan rate of 5 mV s^{-1} to investigate the electrocatalytic behavior of the PEG-WO_3-NiO catalyst systems. As illustrated in Figure 5a, the $PWNiO_{1.5}$ electrocatalyst demonstrates superior OER performance, achieving an overpotential of 349.7 mV at a current density of 10 mA cm^{-2}. When compared to other electrocatalysts, i.e., $PWNiO_{0.5}$ (379.1 mV) and $PWNiO_1$ (378.1 mV), $PWNiO_{1.5}$ exhibits significantly enhanced electrocatalytic activity under identical experimental conditions. This improvement in catalytic efficiency can be attributed to the increasing concentration of Ni within the composite, suggesting a direct correlation between Ni content and performance enhancement. To further investigate the influence of the electrocatalyst composition on reaction kinetics, the Tafel slopes were analyzed, as shown in Figure 5b. The measured Tafel slope values for $PWNiO_{0.5}$, $PWNiO_1$, and $PWNiO_{1.5}$ were 82.3, 79.2, and 71.2 mV dec^{-1}, respectively. Notably, $PWNiO_{1.5}$ exhibited the lowest Tafel slope, indicating improved charge transfer kinetics, which aligns with its lower overpotential, as depicted in Figure 5c. The Tafel dynamic analysis revealed that the $PWNiO_{1.5}$ electrocatalyst exhibits a Tafel slope of 71.2 mV dec^{-1}, signifying that the RDS in the OER is linked to the conversion of Ni–O species into Ni–OOH [39]. The intrinsic electrocatalytic activity of the synthesized samples

was further evaluated through the calculation of the turnover frequency (TOF). TOF values were derived from the integrated charge associated with the reduction peak areas at 300 mV fixed potential, as illustrated in Figure S3a–c [40,41]. Among the investigated samples, the $PWNiO_{1.5}$ catalyst exhibits the highest TOF value of 5.6×10^{-4} s^{-1}, substantially superior those of $PWNiO_{0.5}$ (1.0×10^{-4} s^{-1}) and $PWNiO_1$ (1.7×10^{-4} s^{-1}), as depicted in Figure 5d. The enhanced TOF of $PWNiO_{1.5}$ reflects a greater density of accessible active sites and a more efficient catalytic turnover, thus confirming its superior OER kinetics. These findings promotes faster oxygen evolution per active site and contribute significantly to the overall electrocatalytic enhancement.

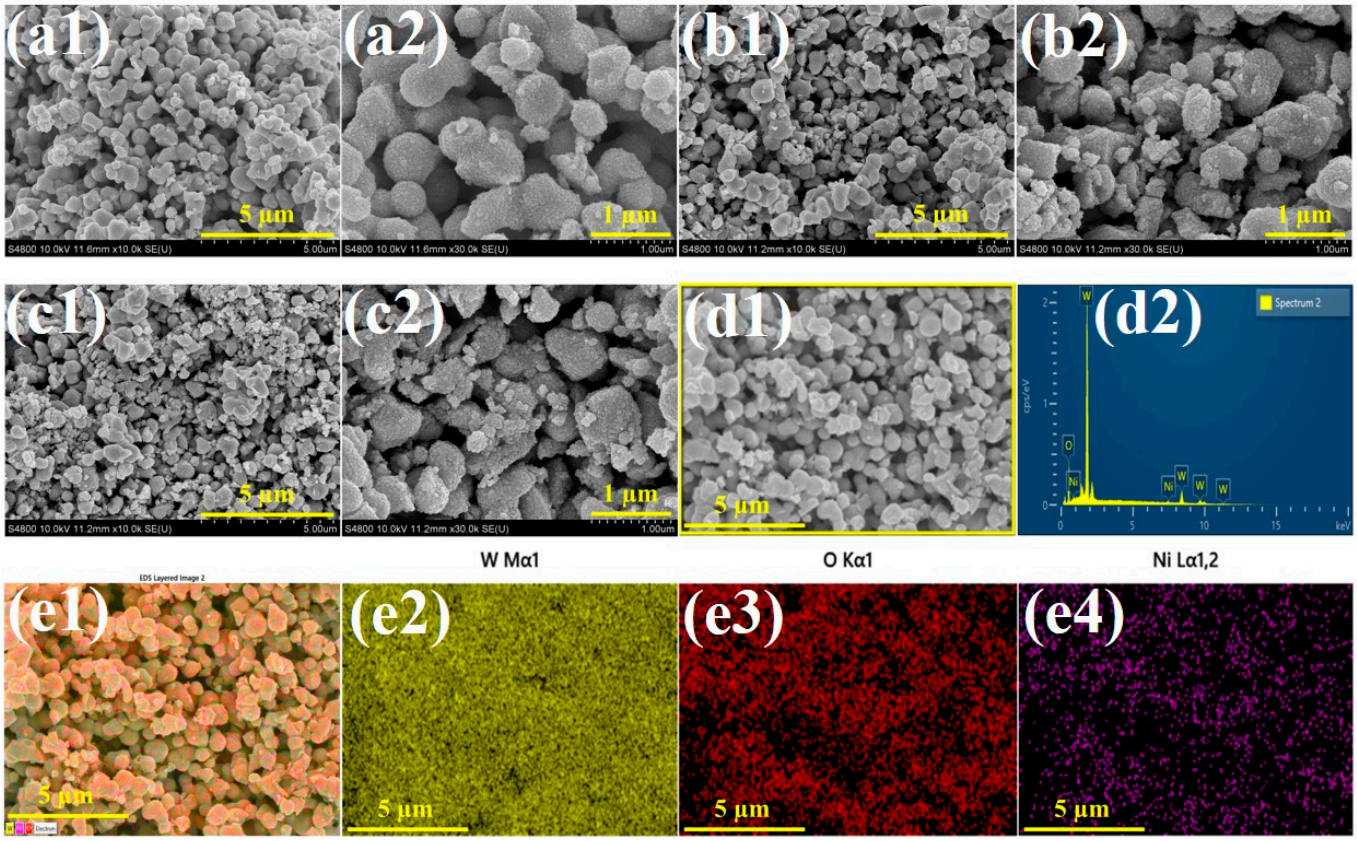

Figure 4. SEM micrograph images of (**a1**,**a2**) $PWNiO_{0.5}$, (**b1**,**b2**) $PWNiO_1$, and (**c1**,**c2**) $PWNiO_{1.5}$. (**d1**,**d2**) Energy-dispersive X-ray spectroscopy analysis of $PWNiO_{1.5}$, and (**e1**–**e4**) elemental mapping data of $PWNiO_{1.5}$ electrocatalyst.

Electrochemical impedance spectroscopy (EIS) was utilized to evaluate the charge transfer kinetics involved in OER, as depicted in Figure 6a. To achieve a more precise understanding of the electrochemical characteristics, the EIS data were fitted to equivalent circuit models. The charge transfer resistance (R_{ct}) values for $PWNiO_{0.5}$, $PWNiO_1$, and $PWNiO_{1.5}$ were determined to be 18.5, 14.7, and 9.7 Ω, respectively. The lower R_{ct} value of $PWNiO_{1.5}$ signifies enhanced charge transport capabilities for OER processes. A reduced R_{ct} reflects an accelerated electron transfer rate at the electrode–electrolyte interface which is crucial for optimizing the overall catalytic activity. Figure S4 presents the cyclic voltammetry (CV) curves for various PEG-WO_3-NiO ratios at different scan rates along with a corresponding plot of current density versus potential. The CV analysis indicates that an increase in scan rate results in a higher current density highlighting the dependence of electrochemical activity on scan rate variations. To further investigate the correlation between electrocatalytic performance and active sites, the electrochemically active surface area (ECSA) was estimated based on the double-layer capacitance (C_{dl}), as depicted in

Figure 6b and $2C_{dl}$ in Figure S5. As shown in Figure 6b, the C_{dl} values for $PWNiO_{0.5}$, $PWNiO_1$, and $PWNiO_{1.5}$ were determined to be 0.95, 1.86, and 2.53 mF cm^{-2}, respectively. Correspondingly, the calculated ECSA values illustrated in Figure 6c were 23.75, 46.62, and 63.25 cm^2 for $PWNiO_{0.5}$, $PWNiO_1$, and $PWNiO_{1.5}$, respectively. The significant enhancement in ECSA with increasing Ni content suggests that the optimized incorporation of Ni effectively enhances the active sites of V, which play a pivotal role in improving the overall electrochemical performance for the OER [42].

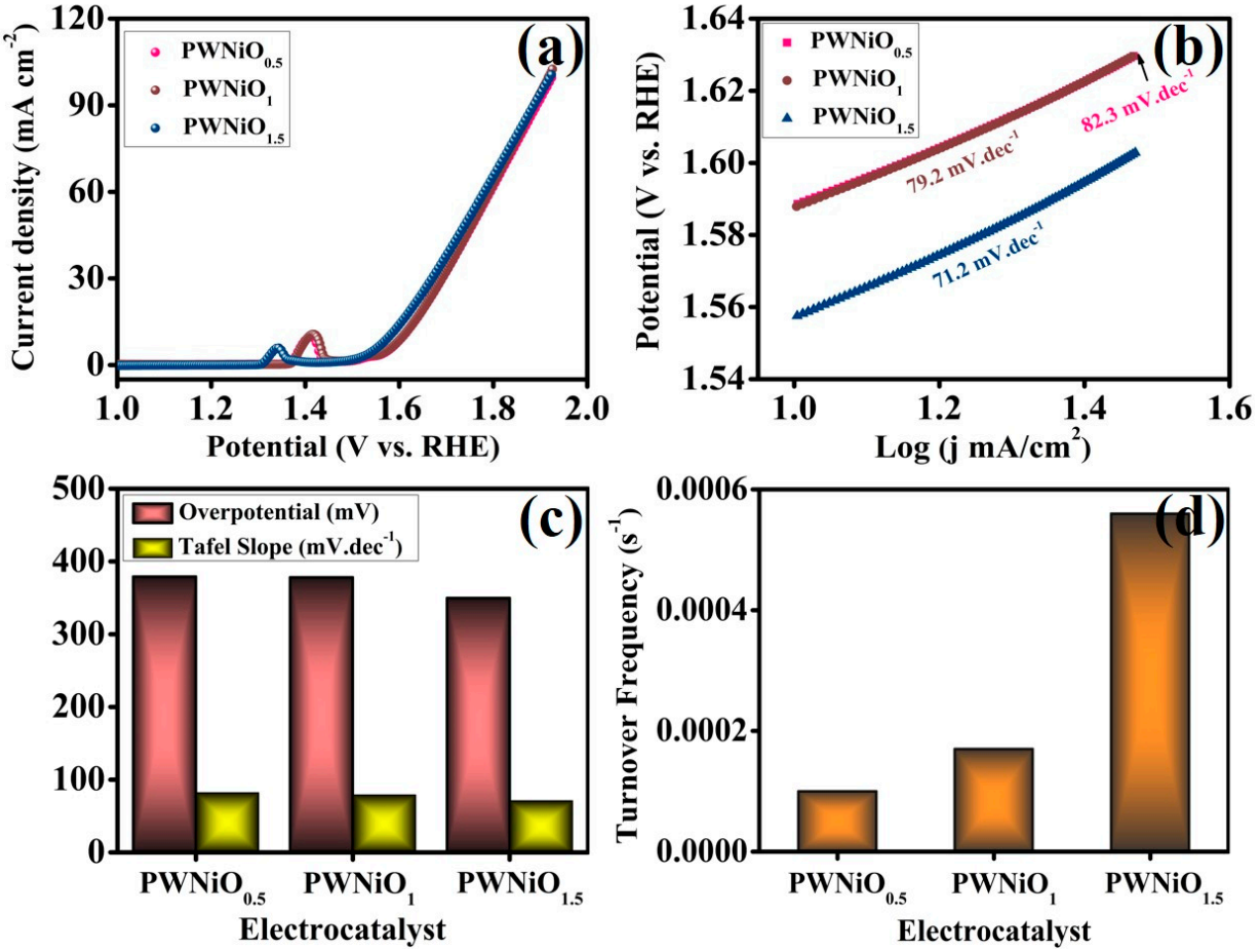

Figure 5. Electrochemical characterizations of electrocatalyst OER performance: (**a**) LSV curves at a 5 mV/s scan rate, (**b**) analogous Tafel slopes, (**c**) assessment of the OER performance concerning overpotential at 10 mA cm^{-2} and Tafel slope, and (**d**) turnover frequency results.

The long-term stability of electrocatalysts is a crucial factor in electrochemical performance evaluation, particularly for potential commercial applications. To assess the structural and electrochemical durability of the heterostructured $PWNiO_{1.5}$ electrocatalyst in a 1.0 M KOH electrolyte, cyclic voltammetry (CV) studies and chronopotentiometry measurements were conducted. The CV cycling test was performed at a scan rate of 50 mV s^{-1} in a 1.0 M KOH electrolyte to monitor the durability of the electrocatalyst under prolonged operational conditions. As depicted in Figure 7a, the polarization curve of $PWNiO_{1.5}$ was recorded before and after 5000 CV cycles to analyze its performance retention. After undergoing 5000 cycles, the electrocatalyst maintained an overpotential of 370.3 mV at a current density of 10 mA cm^{-2} which closely matches the initial values obtained before cycling, demonstrating excellent electrochemical stability. Furthermore, a chronopotentiometry experiment was conducted at a current density of 10 mA cm^{-2} over a continuous 7000 s (Figure 7b) to further examine the catalyst's endurance. The $PWNiO_{1.5}$ electrocatalyst

exhibited remarkable stability. However, a slight loss in performance could be attributed to several factors, including the minor leaching of active materials from the electrode's surface, inadequate diffusion of generated O_2 away from the reaction interface, or potential structural degradation due to oxidation under high potentials [27,43].

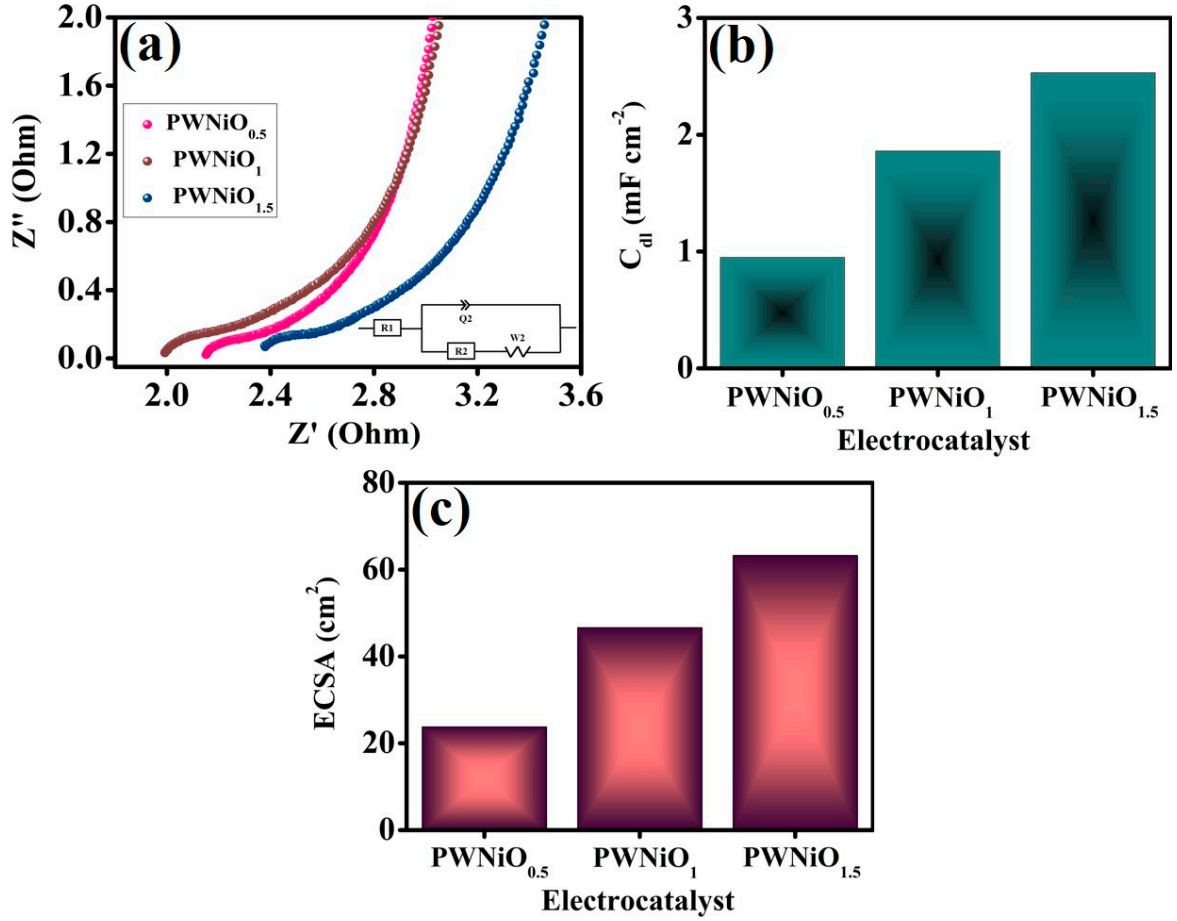

Figure 6. (**a**) EIS spectra, (**b**) C_{dl}, and (**c**) ECSA results of all of the electrocatalysts.

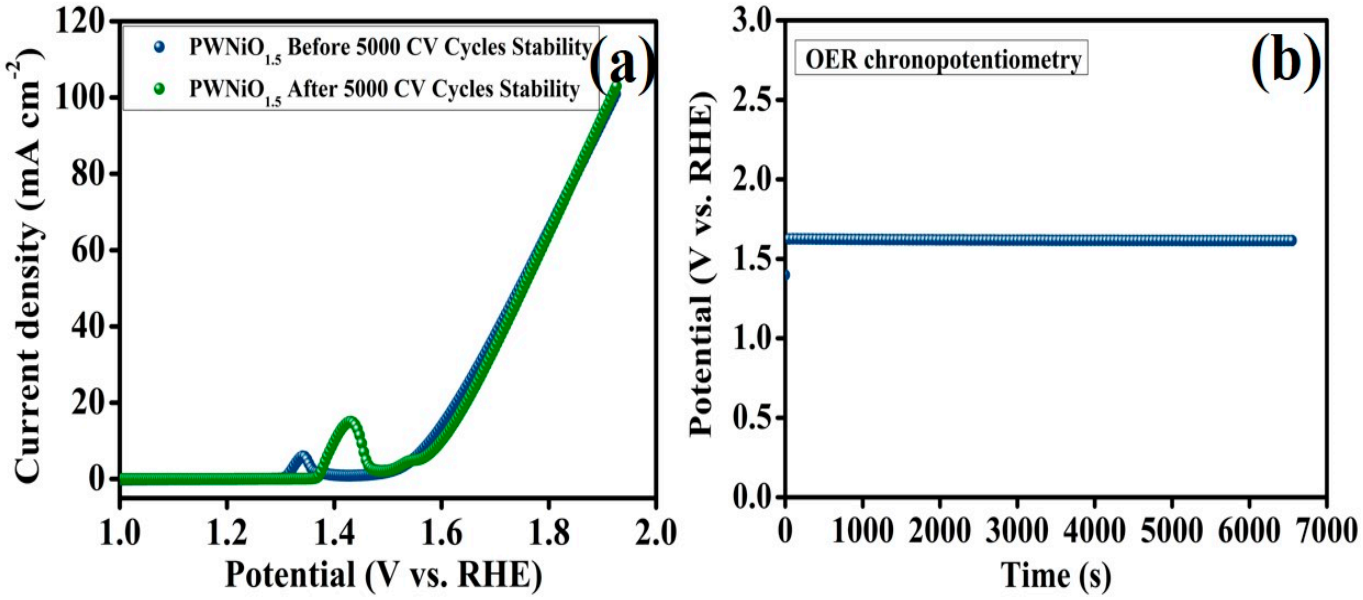

Figure 7. (**a**) LSV curves of $PWNiO_{1.5}$ before and after 5000 CV cycles and (**b**) chronopotentiometry analysis.

4. Conclusions

A PEG-WO_3-NiO electrocatalyst was successfully synthesized via a co-precipitation technique demonstrating promising potential for OER applications. In the PEG-WO_3-NiO composite, NiO nanoparticles are well-integrated within the PEG-WO_3 matrix, forming a homogeneous and uniform dispersion which plays a crucial role in enhancing its electrocatalytic activity. Among the various synthesized compositions, $PWNiO_{1.5}$ exhibited the most outstanding electrocatalytic performance, requiring a relatively low overpotential of 349.7 mV to achieve a current density of 10 mA cm^{-2}. This superior activity can be attributed to the synergistic interactions between the NiO nanoparticles and the PEG-WO_3 structure which enhance electron transport and catalytic activity. Additionally, all of the PWNiO composites displayed reduced charge transfer resistance, facilitating rapid electron and OH^- ion transport across the electrode interface, which is crucial for achieving efficient OER kinetics. This study provides an effective strategy for the fabrication of high-performance electrocatalysts with improved charge transfer dynamics and enhanced electrochemical efficiency. The findings suggest that PEG-WO_3-NiO-based materials hold significant promise for practical electrochemical applications, particularly in energy conversion and storage systems.

Supplementary Materials: The following supporting information can be downloaded at: https://www.mdpi.com/article/10.3390/polym17091281/s1, Figure S1: (a,b) SEM micrograph images of WO_3. Figure S2: (a,b) HRTEM images of $PWNiO_{1.5}$ composite. Figure S3: Reduction areas of (a) $PWNiO_{0.5}$ (b) $PWNiO_1$, and (c) $PWNiO_{1.5}$ electrocatalysts from their corresponding CV for OER TOF. Figure S4: Cyclic voltammetry analysis of all the electrocatalysts at different scan rate. Figure S5: $2C_{dl}$ graph of all the electrocatalysts. Table S1: Comparison of our ternary electro catalysts OER performance result with other reported electrocatalysts. References [21–23,44–51] are cited in the supplementary materials.

Author Contributions: M.B.: Writing—original draft, Methodology, Investigation. P.J.M.: Writing—review and editing, Software. R.U.A.: Software and formal analysis. C.-W.J.: Supervision, Writing—review and editing, Project administration, Funding acquisition. All authors have read and agreed to the published version of the manuscript.

Funding: This research did not receive any specific grant from funding agencies in the public, commercial, or not-for-profit sectors.

Institutional Review Board Statement: Not applicable.

Data Availability Statement: The original contributions presented in the study are included in the article/Supplementary Material, further inquiries can be directed to the corresponding author.

Conflicts of Interest: The authors declare no conflicts of interest.

References

1. Arumugam, B.; Siddharthan, E.E.; Mannu, P.; Thapa, R.; Dong, C.-L.; Jeffery, A.A.; Kim, S.-C. Regulating the electronic structure of $CoMoO_4$ *via* La doping for efficient and durable electrochemical water splitting reactions. *J. Mater. Chem. A* **2025**, *13*, 6749–6767. [CrossRef]
2. Jang, J.-H.; Jeffery, A.A.; Min, J.; Jung, N.; Yoo, S.J. Emerging carbon shell-encapsulated metal nanocatalysts for fuel cells and water electrolysis. *Nanoscale* **2021**, *13*, 15116–15141. [CrossRef] [PubMed]
3. Bockris, J.O. The origin of ideas on a hydrogen economy and its solution to the decay of the environment. *Int. J. Hydrogen Energy* **2002**, *27*, 731–740. [CrossRef]
4. Teli, A.M.; Mane, S.M.; Beknalkar, S.A.; Mishra, R.K.; Jeon, W.; Shin, J.C. Development of Electrochemical Water Splitting with Highly Active Nanostructured NiFe Layered Double Hydroxide Catalysts: A Comprehensive Review. *Catalysts* **2025**, *15*, 293. [CrossRef]
5. Khalid, N.; Rehman, A.; Pervaiz, E. Electrochemical pathway to enhanced water splitting efficiency through cobalt Phosphide-MOFs hybrid. *Int. J. Hydrogen Energy* **2024**, *73*, 231–256. [CrossRef]

6. Xue, R.; Deng, R.; Li, Y.; Gao, M.; Wang, J.; Zhang, Q. Deep eutectic solvent-induced controllable synthesis of bifunctional Ni–Fe–P catalysts for electrochemical water splitting. *Green Chem. Eng.* **2025**, *6*, 93–101. [CrossRef]
7. Greeley, J.; Jaramillo, T.F.; Bonde, J.; Chorkendorff, I.; Nørskov, J.K. Computational high-throughput screening of electrocatalytic materials for hydrogen evolution. *Nat. Mater.* **2006**, *5*, 909–913. [CrossRef]
8. Li, R.; Fan, W.; Rao, P.; Luo, J.; Li, J.; Deng, P.; Wu, D.; Huang, W.; Jia, C.; Liu, Z.; et al. Multimetallic Single-Atom Catalysts for Bifunctional Oxygen Electrocatalysis. *ACS Nano* **2023**, *17*, 18128–18138. [CrossRef]
9. Wondimu, T.H.; Bayeh, A.W.; Kabtamu, D.M.; Xu, Q.; Leung, P.; Shah, A.A. Recent progress on tungsten oxide-based materials for the hydrogen and oxygen evolution reactions. *Int. J. Hydrogen Energy* **2022**, *47*, 20378–20397. [CrossRef]
10. Chae, M.J.; Jung, H.Y.; Suh, S.J. Cyclic Voltammetry-Assisted enhancement of water splitting activity in nanostructured WO_3 catalysts through structural evolution and Pt substitution. *Appl. Surf. Sci.* **2024**, *680*, 161304. [CrossRef]
11. Sharma, L.; Kumar, P.; Halder, A. Phase and Vacancy Modulation in Tungsten Oxide: Electrochemical Hydrogen Evolution. *ChemElectroChem* **2019**, *6*, 3420–3428. [CrossRef]
12. Sekar, S.; Ahmed, A.T.A.; Pawar, S.M.; Lee, Y.; Im, H.; Kim, D.Y.; Lee, S. Enhanced water splitting performance of biomass activated carbon-anchored WO_3 nanoflakes. *Appl. Surf. Sci.* **2020**, *508*, 145127. [CrossRef]
13. Hu, G.; Li, J.; Liu, P.; Zhu, X.; Li, X.; Ali, R.N.; Xiang, B. Enhanced electrocatalytic activity of WO_3@NPRGO composite in a hydrogen evolution reaction. *Appl. Surf. Sci.* **2018**, *463*, 275–282. [CrossRef]
14. Yu, S.; Yu, X.; Yang, H.; Li, F.; Li, S.; Kang, Y.S.; Zheng, J.Y. Mechanism, modification and stability of tungsten oxide-based electrocatalysts for water splitting: A review. *J. Energy Chem.* **2024**, *99*, 23–49. [CrossRef]
15. Liu, F.; Feng, Z.; Zhang, X.; Cui, L.; Liu, J. One-step achievement of Fe-doped and interfacial Ru nanoclusters co-engineered $Ni(OH)_2$ electrocatalyst on Ni foam for promoted oxygen evolution reaction. *J. Colloid Interface Sci.* **2023**, *638*, 498–505. [CrossRef]
16. Li, Y.; Bao, X.; Chen, D.; Wang, Z.; Dewangan, N.; Li, M.; Xu, Z.; Wang, J.; Kawi, S.; Zhong, Q. A Minireview on Nickel-Based Heterogeneous Electrocatalysts for Water Splitting. *ChemCatChem* **2019**, *11*, 5913–5928. [CrossRef]
17. Kitiphatpiboon, N.; Chen, M.; Li, X.; Liu, C.; Li, S.; Wang, J.; Peng, S.; Abudula, A.; Guan, G. Heterointerface engineering of Ni_3S_2@NiCo-LDH core-shell structure for efficient oxygen evolution reaction under intermittent conditions. *Electrochim. Acta* **2022**, *435*, 141438. [CrossRef]
18. Zeng, J.; Chen, L.; Li, L.; Yang, W.; Zou, H.; Chen, S. Effect of PEG on Performance of NiMnO Catalyst for Hydrogen Evolution Reaction. *Front. Chem.* **2020**, *8*, 281. [CrossRef]
19. Babar, P.; Lokhande, A.; Gang, M.; Pawar, B.; Pawar, S.; Kim, J.H. Thermally oxidized porous NiO as an efficient oxygen evolution reaction (OER) electrocatalyst for electrochemical water splitting application. *J. Ind. Eng. Chem.* **2018**, *60*, 493–497. [CrossRef]
20. Chen, Y.; Rui, K.; Zhu, J.; Dou, S.X.; Sun, W. Recent Progress on Nickel-Based Oxide/(Oxy)Hydroxide Electrocatalysts for the Oxygen Evolution Reaction. *Chem. A Eur. J.* **2019**, *25*, 703–713. [CrossRef]
21. Manjunath, V.; Bimli, S.; Biswas, R.; Didwal, P.N.; Haldar, K.K.; Mahajan, M.; Deshpande, N.G.; Bhobe, P.A.; Devan, R.S. Experimental investigations on morphology controlled bifunctional NiO nano-electrocatalysts for oxygen and hydrogen evolution. *Int. J. Hydrogen Energy* **2022**, *47*, 39018–39029. [CrossRef]
22. Mondal, A.; Paul, A.; Srivastava, D.N.; Panda, A.B. NiO hollow microspheres as efficient bifunctional electrocatalysts for Overall Water-Splitting. *Int. J. Hydrogen Energy* **2018**, *43*, 21665–21674. [CrossRef]
23. Shaghaghi, Z.; Akbari, S. Hydrogen and oxygen production on Ag_2O/NiO hybrid nanostructures via electrochemical water splitting. *Int. J. Hydrogen Energy* **2023**, *51*, 936–949. [CrossRef]
24. Pan, U.N.; Singh, T.I.; Paudel, D.R.; Gudal, C.C.; Kim, N.H.; Lee, J.H. Covalent doping of Ni and P on 1T-enriched MoS_2 bifunctional 2D-nanostructures with active basal planes and expanded interlayers boosts electrocatalytic water splitting. *J. Mater. Chem. A* **2020**, *8*, 19654–19664. [CrossRef]
25. Guo, J.; Wei, Z.; Wang, K.; Zhang, H. Synergistic coupling of CoFe-layered double hydroxide nanosheet arrays with reduced graphene oxide modified Ni foam for highly efficient oxygen evolution reaction and hydrogen evolution reaction. *Int. J. Hydrogen Energy* **2021**, *46*, 27529–27542. [CrossRef]
26. Wang, P.; Yu, Y.; Yan, Y.; Qin, B.; Ye, Z.; Zhong, W.; Cai, W.; Zheng, X. N plasma assisted Fe doped NiCo nanosheet arrays for alkaline electrocatalytic oxygen evolution. *J. Alloys Compd.* **2023**, *941*, 168954. [CrossRef]
27. Tang, C.; Zhong, L.; Xiong, R.; Xiao, Y.; Cheng, B.; Lei, S. Regulable in-situ autoredox for anchoring synergistic Ni/NiO nanoparticles on reduced graphene oxide with boosted alkaline electrocatalytic oxygen evolution. *J. Colloid Interface Sci.* **2023**, *648*, 181–192. [CrossRef]
28. Bhosale, M.; Thangarasu, S.; Magdum, S.S.; Jeong, C.; Oh, T.-H. Enhancing the electrocatalytic performance of vanadium oxide by interface interaction with rGO and NiO nanostructures for electrochemical water oxidation. *Int. J. Hydrogen Energy* **2023**, *54*, 1449–1460. [CrossRef]
29. Mohan, L.; Avani, A.; Kathirvel, P.; Marnadu, R.; Packiaraj, R.; Joshua, J.R.; Nallamuthu, N.; Shkir, M.; Saravanakumar, S. Investigation on structural, morphological and electrochemical properties of Mn doped WO_3 nanoparticles synthesized by co-precipitation method for supercapacitor applications. *J. Alloys Compd.* **2021**, *882*, 160670. [CrossRef]

30. Morankar, P.J.; Amate, R.U.; Chavan, G.T.; Teli, A.M.; Dalavi, D.S.; Jeon, C.-W. Improved electrochromic performance of potentiostatically electrodeposited nanogranular WO_3 thin films. *J. Alloys Compd.* **2023**, *945*, 169363. [CrossRef]
31. Balčiūnaitė, A.; Upadhyay, K.K.; Radinović, K.; Santos, D.M.F.; Montemor, M.F.; Šljukić, B. Steps towards highly-efficient water splitting and oxygen reduction using nanostructured β-$Ni(OH)_2$. *RSC Adv.* **2022**, *12*, 10020–10028. [CrossRef] [PubMed]
32. Guo, Z.; Wang, X.; Gao, Y.; Liu, Z. Co/Cu-modified NiO film grown on nickel foam as a highly active and stable electrocatalyst for overall water splitting. *Dalton Trans.* **2020**, *49*, 1776–1784. [CrossRef] [PubMed]
33. He, W.; Li, W.; Liu, J.; Lou, G.; Zhang, C.; Liu, Y.; Li, J. Controlling crystallographic orientation in h-WO_3 films to maximize photoelectrochemical water splitting efficiency. *J. Mater. Chem. A* **2025**, *13*, 7284–7294. [CrossRef]
34. Baby, N.; Murugan, N.; Thangarasu, S.; Kim, Y.A.; Oh, T.-H. Synergistic insights into the electrocatalytic mechanisms of ZIF-derived Co_3S_4 on 1T-WS_2/WO_3 for electrochemical water splitting. *Int. J. Hydrogen Energy* **2024**, *94*, 1005–1017. [CrossRef]
35. Morankar, P.J.; Amate, R.U.; Teli, A.M.; Beknalkar, S.A.; Jeon, C.-W. Exploring electrochromic performance via layered deposition of tungsten oxide on niobium oxide composite electrode. *J. Power Sources* **2024**, *613*, 234930. [CrossRef]
36. Liu, J.; Zheng, Y.; Jiao, Y.; Wang, Z.; Lu, Z.; Vasileff, A.; Qiao, S. NiO as a Bifunctional Promoter for RuO_2 toward Superior Overall Water Splitting. *Small* **2018**, *14*, e1704073. [CrossRef]
37. Hu, Q.; Li, W.; Abouelamaiem, D.I.; Xu, C.; Jiang, H.; Han, W.; He, G. Hollow Cu-doped NiO microspheres as anode materials with enhanced lithium storage performance. *RSC Adv.* **2019**, *9*, 20963–20967. [CrossRef]
38. Yu, M.; Budiyanto, E.; Tüysüz, H. Principles of water electrolysis and recent progress in cobalt-, nickel-, and iron-based oxides for the oxygen evolution reaction. *Angew. Chem. Int. Ed.* **2022**, *61*, e202103824. [CrossRef]
39. Zhai, Y.; Ren, X.; Sun, Y.; Li, D.; Wang, B.; Liu, S. Synergistic effect of multiple vacancies to induce lattice oxygen redox in NiFe-layered double hydroxide OER catalysts. *Appl. Catal. B Environ.* **2022**, *323*, 122091. [CrossRef]
40. Roy, S.S.; Karmakar, A.; Madhu, R.; Nagappan, S.; Dhandapani, H.N.; Kundu, S. Three-Dimensional Sm-Doped NiCu-LDH on Ni Foam as a Highly Robust Bifunctional Electrocatalyst for Total Water Splitting. *ACS Appl. Energy Mater.* **2023**, *6*, 8818–8829. [CrossRef]
41. Pitchai, C.; Chen, C.-M. Electrochemically enhanced oxygen evolution and urea oxidation reactions with advanced high-entropy LDH nanoneedles. *Sustain. Energy Fuels* **2025**, *9*, 1829–1838. [CrossRef]
42. Hanan, A.; Shu, D.; Aftab, U.; Cao, D.; Laghari, A.J.; Solangi, M.Y.; Abro, M.I.; Nafady, A.; Vigolo, B.; Tahira, A.; et al. Co_2FeO_4@rGO composite: Towards trifunctional water splitting in alkaline media. *Int. J. Hydrogen Energy* **2022**, *47*, 33919–33937. [CrossRef]
43. Ma, L.; Sui, S.; Zhai, Y. Preparation and characterization of Ir/TiC catalyst for oxygen evolution. *J. Power Sources* **2008**, *177*, 470–477. [CrossRef]
44. Jo, S.G.; Kim, C.-S.; Kim, S.J.; Lee, J.W. Phase-Controlled NiO Nanoparticles on Reduced Graphene Oxide as Electrocatalysts for Overall Water Splitting. *Nanomaterials* **2021**, *11*, 3379. [CrossRef]
45. Wang, C.P.; Kong, L.J.; Sun, H.; Zhong, M.; Cui, H.J.; Zhang, Y.H.; Wang, D.H.; Zhu, J.; Bu, X.H. Carbon Layer Coated Ni_3S_2/MoS_2 Nanohybrids as Efficient Bifunctional Electrocatalysts for Overall Water Splitting. *ChemElectroChem* **2019**, *6*, 5603–5609. [CrossRef]
46. Tian, L.; Liu, H.; Zhang, B.; Liu, Y.; Lv, S.; Pang, L.; Li, J. Ni and CeO_2 Nanoparticles Anchored on Cicada-Wing-like Nitrogen-Doped Porous Carbon as Bifunctional Catalysts for Water Splitting. *ACS Appl. Nano Mater.* **2021**, *5*, 1252–1262. [CrossRef]
47. Liang, D.; Zhang, H.; Ma, X.; Liu, S.; Mao, J.; Fang, H.; Yu, J.; Guo, Z.; Huang, T. MOFs-derived core-shell Co_3Fe_7@Fe_2N nanopaticles supported on rGO as high-performance bifunctional electrocatalyst for oxygen reduction and oxygen evolution reactions. *Mater. Today Energy* **2020**, *17*, 100433. [CrossRef]
48. Upadhyay, S.; Mir, R.A.; Pandey, O.P. $Ni(OH)_2$ nanosheets and highly stable $Ni(OH)_2$/GO nanocomposite for its improved OER performance. *Int. J. Hydrogen Energy* **2023**, *48*, 36687–36693. [CrossRef]
49. Sprengel, S.; Amiri, M.; Bezaatpour, A.; Nouhi, S.; Baues, S.; Wittstock, G.; Wark, M. One-Pot Synthesis of Ni-MOF/Co-MOF Hybrid as Electrocatalyst for Oxygen Evolution Reaction. *J. Electrochem. Soc.* **2022**, *169*, 124504. [CrossRef]
50. Sreekanth, T.; Dillip, G.; Nagajyothi, P.; Yoo, K.; Kim, J. Integration of Marigold 3D flower-like Ni-MOF self-assembled on MWCNTs via microwave irradiation for high-performance electrocatalytic alcohol oxidation and oxygen evolution reactions. *Appl. Catal. B Environ.* **2021**, *285*, 119793. [CrossRef]
51. Wu, Z.-Y.; Ji, W.-B.; Hu, B.-C.; Liang, H.-W.; Xu, X.-X.; Yu, Z.-L.; Li, B.-Y.; Yu, S.-H. Partially oxidized Ni nanoparticles supported on Ni-N co-doped carbon nanofibers as bifunctional electrocatalysts for overall water splitting. *Nano Energy* **2018**, *51*, 286–293. [CrossRef]